







Cite this: *Phys. Chem. Chem. Phys.*,
2019, 21, 14440

Energy- and conformer-dependent excited-state relaxation of an *E/Z* photoswitchable thienyl-ethene†

Jamie D. Young,‡ Chana R. Honick,‡ Jiawang Zhou,  § Cody R. Pitts,¶
Fereshte Ghorbani, Garvin M. Peters,  Thomas Lectka, John D. Tovar  and
Arthur E. Bragg  *

Bis(bithienyl)-1,2-dicyanoethene (4TCE) is a photoswitch that operates via reversible *E/Z* photoisomerization following absorption of visible light. *cis*-to-*trans* photoisomerization of 4TCE requires excitation below 470 nm, is relatively inefficient (quantum yield < 5%) and occurs via the lowest-lying triplet. We present excitation-wavelength dependent (565–420 nm) transient absorption (TA) studies to probe the photophysics of *cis*-to-*trans* isomerization to identify sources of switching inefficiency. TA data reveals contributions from more than one switch conformer and relaxation cascades between multiple states. Fast (~4 ps) and slow (~40 ps) components of spectral dynamics observed at low excitation energies (>470 nm) are readily attributed to deactivation of two conformers; this assignment is supported by computed thermal populations and absorption strengths of two molecular geometries (P_A and P_B) characterized by roughly parallel dipoles for the thiophenes on opposite sides of the ethene bond. Only the P_B conformer is found to contribute to triplet population and the switching of *cis*-4TCE: high-energy excitation (<470 nm) of P_B involves direct excitation to S_2 , relaxation from which prepares an ISC-active S_1 geometry (ISC QY 0.4–0.67, $k_{ISC} \sim 1.6\text{--}2.6 \times 10^{-9} \text{ s}^{-1}$) that is the gateway to triplet population and isomerization. We ascribe low *cis*-to-*trans* isomerization yield to excitation of the nonreactive P_A conformer (75–85% loss) as well as losses along the $P_B S_2 \rightarrow S_1 \rightarrow T_1$ cascade (10–20% loss). In contrast, electrocyclization is inhibited by the electronic character of the excited states, as well as a non-existent thermal population of a reactive “antiparallel” ring conformation.

Received 2nd March 2019,
Accepted 13th March 2019

DOI: 10.1039/c9cp01226e

rsc.li/pccp

Introduction

A molecular switch is any molecule that can be driven reversibly and selectively through reactions between two or more chemical states with an external stimulus. Photoswitchable molecules and materials have garnered significant attention in recent years, primarily due to their tantalizing potential for photochromic materials,¹ optical data storage,^{2,3} molecular electronics,^{4–6} photobiology,^{7,8} vision restoration,⁹ molecular machines,¹⁰ and photoresponsive soft materials.¹¹ In addition to exhibiting

desirable spectral characteristics to facilitate selective excitation of each switch state, including sensitivity to visible light¹² and nonoverlapping absorption features,¹³ a photoswitch should be robust and fatigue-resistant to repeated conversions and exhibit thermal stability in each state.¹⁴ Furthermore, fast response times require reasonably high conversion efficiencies (quantum yields) per excitation, with minimal losses through competing deactivation pathways.¹⁵ Hence the design of molecular photoswitches involves the challenge of understanding molecular properties and reactivities in ground and excited states,^{16,17} as well as how these properties and reactivities are affected by variations in molecular conformation or changes in chemical environment.⁸

Photocyclizable diarylethenes and *E/Z* photoisomerizing azobenzenes are two prominent classes of photoswitchable compounds that have been explored and exploited extensively in recent years in efforts to design and optimize photoswitches for various chemical, material, and biological applications. Diarylethenes, such as dithienyl perfluorocyclopentene, typically exist as mixtures of two conformers, with the two pendant aryl

Department of Chemistry, Johns Hopkins University, 3400 N. Charles St, Baltimore, MD 21218, USA. E-mail: artbragg@jhu.edu

† Electronic supplementary information (ESI) available: Additional transient absorption spectra, their spectral analyses, and computed absorption spectra. See DOI: 10.1039/c9cp01226e

‡ These authors have contributed equally to the preparation of this work.

§ Present address: Department of Chemistry, Northwestern University, 2145 Sheridan Rd, Evanston, IL 60208, USA.

¶ Present address: ETH Zürich, Department of Chemistry and Applied Biosciences, Vladimir-Prelog-Weg 2, 8093 Zürich, Switzerland.

rings roughly oriented either in mirror or C_2 symmetry, known as 'parallel' and 'anti-parallel' geometries, respectively.² Photo-switching of these compounds *via* 6π -electrocyclization is only possible from the antiparallel conformation by symmetry^{18,19} (*i.e.* *via* a conrotatory cyclization²⁰); thus, in the absence of external factors that control the conformational distribution of an ensemble (*e.g.* molecular packing, as in crystals,³ or by incorporation into polymers²¹), the quantum yield for cyclization is limited intrinsically. Significant research has sought to overcome this limit and produce diarylethenes that can be cyclized reliably in numerous applications.^{2,3,18} Azobenzenes on the other hand undergo *E/Z* photoisomerization, and the larger geometrical change associated with azobenzenes has resulted in their incorporation into several important biomolecular applications.²² However, compared to diarylethenes, azobenzenes traditionally have photochemical limitations, including thermal instability of the *cis* isomer²³ and chemical instability leading to the formation of undesirable photoproducts.

Guo *et al.*²⁴ and Zhou *et al.*²⁵ previously reported the design, synthesis, and photophysical characterization of bis(bithienyl)-1,2-dicyanoethene (4TCE), a diarylethene that switches solely through *E/Z* isomerization rather than electrocyclization, much more like azobenzenes than structurally related dithienyl ethenes. Chart 1 presents the structure of 4TCE along with related molecules investigated in this work; Fig. 1 presents their steady-state absorption spectra. While the *E/Z* activity of this switch was attributed principally to the α -linkage of the pendant thienyl groups to the ethene core, the incorporation of the electron-deficient cyano-substituents on the core and secondary thienyl groups at the periphery introduces a significant push-pull charge-transfer effect across the chromophore, giving rise to electronic transitions that are much lower in energy than the near-UV transitions of most diarylethenes (*cf.* Fig. 1, structures 1 and 2 *vs.* 3). This CT character appears to shut down the possibility for photocyclization, which has been observed in β -linked dithienyl perfluorocyclopentenes, thereby allowing reversible *E/Z* isomerization to dominate the photochemistry.

Hence, 4TCE presents a new entry in the palette of *E/Z* isomerizing photoswitches and exhibits many favorable properties relative to most azobenzenes, including no formation of undesirable photoproducts, thermal stability of both *cis* and *trans* isomers, and sensitivity to visible light absorption with relatively high photostationary yields for isomerization and fatigue resistance. *trans*-4TCE is ~ 4 kcal mol⁻¹ more energetically stable than the *cis*-isomer and, based on our previous calculations,

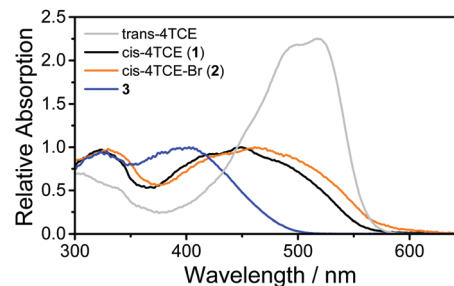


Fig. 1 Steady-state UV/Vis absorption spectra for *trans*-4TCE (grey), *cis*-4TCE ((1) black), *cis*-4TCE-Br ((2) orange) and the bis(bithienyl)perfluorocyclopentene ((3) – blue). Spectra for 1–3 are normalized to peak intensity; *trans*- and *cis*-4TCE are presented at relative absorptivities.

there exists a > 27 kcal mol⁻¹ potential energy barrier between isomers along the S_0 surface.^{24,25} However, *trans*-4TCE readily isomerizes upon exposure to low intensity room lights to achieve $\sim 100\%$ *E-to-Z* conversion. The reverse process can be accomplished with blue light (< 440 nm, $\sim 60\%$) or by heating (> 80 °C, 100% conversion). 4TCE has potential for switching applications that require large-scale structural modifications, as a result of the large geometry change associated with isomerization following irradiation with visible light.

Our previous photophysical characterization of 4TCE revealed a novel and potentially exploitable exclusivity in its photoisomerization mechanisms.²⁵ Specifically, switching was found to occur by electronic relaxation through mutually exclusive manifolds of spin multiplicity for each isomerization reaction: *trans-to-cis* isomerization only occurs *via* electronic relaxation within the singlet manifold. In contrast, *cis-to-trans* isomerization is only observed following excitation with light below 460 nm which results in a relaxation cascade to a triplet state from which isomerization occurs. Interesting questions that remain include why the quantum yield for isomerization from the *cis* isomer is so low compared to that for the *trans* isomer following 420 nm excitation ($\sim 5\%$ *cis-to-trans* *vs.* 23% *trans-to-cis*), and therefore what structural modifications could be made to improve the performance of this switch.

Here we present a deeper investigation of excited-state relaxation mechanisms exhibited by *cis*-4TCE as a function of excitation energy and in comparison with dynamics of related chromophore structures in order to better understand both the relaxation pathways available to excited *cis*-4TCE and to understand why this diarylethene photoswitch seemingly isomerizes so inefficiently (*i.e.* why the quantum yield is so low). Overall, we demonstrate that the efficiency of the *cis-to-trans* isomerization

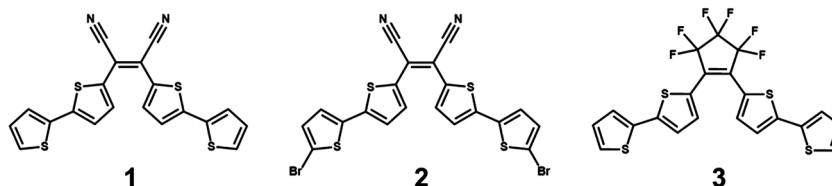


Chart 1 Structures of chromophores studied in this work: (1) *cis*-bis(bithienyl)-1,2-dicyanoethene (4TCE), (2) *cis*-4TCE-Br and (3) bis(bithienyl)-perfluorocyclopentene.

mechanism is limited by both the relative reactivity of 4TCE conformers present at room temperature as well as losses along the photophysical cascade leading to the reactive triplet.

Experimental

Sample preparation

The synthesis of 4TCE was described in detail previously.²⁴ Synthesis of a brominated 4TCE derivative (**2**) also studied in this work was performed as follows: 4TCE (600 mg, 1.5 mmol) and DMF (70 mL) were added to a flame-dried round bottom flask equipped with a stir bar under nitrogen atmosphere. Freshly recrystallized NBS (528 mg, 3.0 mmol) was then added to the reaction mixture. The reaction flask was wrapped with aluminum foil, and the mixture was stirred for 24 h. The crude product was diluted with CH₂Cl₂ and washed with brine. The organic layer was dried over MgSO₄, filtered through Celite, and concentrated. The crude material was purified by column chromatography on silica gel with hexanes:CH₂Cl₂ (1:1) in the dark to prevent conversion of the *trans* form to the *cis* form, which happens rapidly under room lights. Compound **2** was obtained as a deep red solid with a 25% yield. ¹H NMR (400 MHz, CDCl₃): δ 7.75 (d, *J* = 4.0 Hz, 2H), 7.15 (d, *J* = 4.0 Hz, 2H), 7.10 (m, 2H), 7.05 (m, 2H). HRMS (ES⁺): *m/z* calculated 563.7917 for C₂₀H₈Br₂N₂S₄, found 563.7916. ¹H NMR for *cis* form (400 MHz, CDCl₃): δ 7.45 (d, *J* = 4.0 Hz, 2H), 7.10 (d, *J* = 4.0 Hz, 2H), 7.01 (m, 2H), 6.98 (m, 2H).

An analog of 4TCE, 5,5''-(perfluorocyclopent-1-ene-1,2-diyl)di-2,2'-bithiophene (**3**), in which the dicyanoethane is replaced by a perfluorocyclopentene core linked to the α positions of the bithienyl pendants was also studied to further isolate signatures of spectral dynamics associated with relaxation of 4TCE. This compound was synthesized as follows: 2-([2,2'-bithiophen]-5-yl)-4,4,5,5-tetramethyl-1,3,2-dioxaborolane (500 mg, 1.71 mmol), Pd₂(dba)₃·CHCl₃ (14 mg, 0.14 mmol), XPhos (14 mg, 0.28 mmol), and K₃PO₄ (440 mg, 2.05 mmol) were added to a Schlenk flask, which was then evacuated and backfilled with N₂ three times. 1,2-Dichloro-3,3,4,4,5,5-hexafluorocyclopent-1-ene (168 mg, 0.685 mmol) and 1,4-dioxane (10 mL) were then added, and the solution was heated to reflux for 16 hours. The solution was then cooled to room temperature and diluted with 20 mL of diethyl ether, washed twice with 20 mL saturated NH₄Cl, once with 20 mL brine and dried over MgSO₄ before concentrating under reduced pressure. Purification by column chromatography (silica, 95:5 hexanes:DCM) afforded **3** as an orange solid (216 mg, 0.428 mmol, 63%). ¹H NMR (400 MHz, CDCl₃): δ 7.41 (d, 2H, 3.8 Hz), 7.30 (dd, 2H, 5.1 Hz), 7.23 (dd, 2H, 3.6 Hz), 7.19 (d, 2H, 3.8 Hz), 7.03 (dd, 2H, 5.1 Hz). ¹³C (¹H) NMR (100 MHz, CDCl₃): 143.1, 136.1, 133.2, 128.3, 126.2, 125.5, 124.2. ¹⁹F NMR (300 MHz, CDCl₃): δ -110.81 (t, 4F, 5.2 Hz), -131.87 (p, 2F, 5.2 Hz). Internal standard: 1-chloro-3-(trifluoromethyl)benzene (δ -64.22). HRMS (EI): *m/z* calculated 503.9570 for C₂₁H₁₀F₆S₄, found 503.9571.

Solutions of *cis*-4TCE (**1**) or its brominated derivative (**2**) in chlorobenzene (CB, Fisher Scientific, >99% purity) were prepared at concentrations of ~3 × 10⁻⁴ mol dm⁻³ such that

the optical density of the *cis* sample was ~0.5 at peak absorption (~480 nm). Sample solutions were circulated through a 1 mm path-length quartz flow cell whose components are chemically resistant to sample solutions. Exposure to ambient white light drives 100% *E*-to-*Z* conversion of **1** and **2** in solution, as confirmed by NMR. Thus prior to any spectroscopic measurements all samples were exposed to room light to ensure that only the *cis* isomer was the chromophore responsible for observed spectroscopic signatures in transient absorption measurements. UV/Vis spectra were recorded before and after ultrafast measurements using a diode-array spectrometer coupled to tungsten and deuterium light sources (Stellarnet) to monitor sample isomerization and degradation resulting from exposure to ultrafast laser pulses. As with previous investigations, negligible bulk sample conversion was observed over the course of a measurement (~20 minutes per TAS scan) due to simultaneous exposure to overhead lights, and persistent photoproducts were only observed after several days of intensive exposure to laser excitation. Control experiments using pure *trans*-4TCE solutions were run at the longest excitation wavelengths used in this study to verify no contamination of data collected with the *cis*-isomer. Because **3** does not show any evidence of isomerization or cyclization (*i.e.* photoswitching), spectroscopic measurements of **3** were performed using a solution in a 1 mm cuvette.

Ultrafast spectroscopy

Our experimental setup for transient absorption measurements has been described in detail elsewhere;^{26,27} however, for clarity, we note features of the setup that were applicable to the data reported herein. Ultrafast pulses were generated with a commercial regeneratively amplified Ti:sapphire laser system (Coherent Legend Elite, 1 kHz rep. rate, 35 fs pulse duration, 4.0 mJ per pulse). Wavelength tunable pump pulses (~40 fs full-width at half maximum) were generated using an optical parametric amplifier (OPA, Coherent Operasolo), allowing for excitation wavelengths in the range 565–420 nm. Broadband white-light continua spanning 400–1100 nm were generated in either a 2 mm sapphire plate (450–1100 nm) or a 2 mm CaF₂ crystal (400–1075 nm). Pulse energies for all actinic pump wavelengths were attenuated to about 1–5 μJ per pulse for all data presented. In order to eliminate signatures of time-dependent polarization anisotropy from the measured dynamics, the polarization of the white-light probe was set at the magic angle relative to the polarization of the actinic pump using a thin broadband wire-grid polarizer (Thorlabs) placed immediately before the sample. Probe pulses were focused to a spot size of ~50 μm at the sample using an off-axis parabolic reflector; the pump beam was focused to a size of ~1 mm and overlapped with the probe beam at a small angle (<10°) at the sample. The optical path of the pump beam includes a retroreflection from a UV-enhanced aluminum corner-cube mirror; the relative pump-probe pulse delay was controlled by moving the corner cube with a motorized translation stage (Newport). Typical time resolution for these measurements is on the order of 150 fs; temporal fits to absorption transients presented below included a convolution

with the instrument response. Probe light transmitted through the sample was filtered and dispersed onto a multichannel array, and transient spectra were calculated using an acquisition algorithm described previously.

Computational details

Calculations of 4TCE conformer geometries and their minimum energies were performed with the Gaussian 09 package²⁸ using the M052X/6-31G* level of theory.^{29,30} The Polarizable Continuum Model (PCM) was also included to incorporate the effect of the solvent (chlorobenzene). M052X and TD-M052X have been reported previously to yield the best predictions for both structural and spectral parameters of diarylethene derivatives.³¹ All geometry optimizations ignored symmetry constraints. Vibrational analysis at the optimized geometries returned no imaginary frequencies. Time-dependent density functional theory (TD-DFT), also calculated at the M052X level of theory, was used to determine the vertical electronic transition energies ($S_1 \leftarrow S_0$) for each of the isolated conformers.

Results

Fig. 2 presents transient absorption spectra obtained by probing at wavelengths across the visible and near-infrared (<1100 nm) and collected following excitation at both low (530 nm, a) and

high energies (420 nm, b). The time-dependent spectra are presented as spectral waterfall plots at representative time delays. For an alternative perspective that is helpful for tracing the complex spectral dynamics, we present the same data as contour plots in the ESI† (Fig. S1) with vertical axes that are linear in time delay up to 1 ps and logarithmic afterwards, respectively, in order to highlight clearly the evolution of features on multiple timescales following sample excitation.

The TA spectral evolution observed with visible probe wavelengths following 530 nm excitation is similar to what we have observed previously,²⁵ with spectral features assigned as follows: the broad negative feature centered around 525 nm corresponds with bleaching of the ground-state absorption (ground-state bleach, GSB). Stimulated emission (SE) from the photoprepared singlet excited state appears between 550 and 650 nm. An excited-state absorption band appears at each end of the visible range, above 650 nm ("singlet transient absorption" band 1, or STA1) and below 475 nm (STA2); the latter overlaps significantly with the region of the *cis*-4TCE GSB. An additional absorption feature overlooked previously peaks around 575 nm roughly 1 ps after sample excitation (STA3); this feature overlaps significantly with the GSB and SE bands and disappears within 10–20 ps, leaving only signatures of GSB and SE in this region at longer delays. Notably, this is a minor feature with 530 nm excitation but becomes more prominent at higher excitation energies. Finally, transient absorption in the near-infrared (NIR) region of the spectrum (850–1100 nm) was not examined previously; Fig. 2(a) reveals that a low-energy transient absorption feature (STA0) peaks just below 1100 nm and disappears on a timescale commensurate with GSB recovery. Importantly, all spectral features observed following 530 nm excitation disappear (*i.e.* return to the baseline) well within 1 ns.

TAS data collected with higher excitation energy (*e.g.* 420 nm) exhibits many of the same spectral features observed at lower excitation energies, albeit with significantly enhanced contribution from STA3, which overwhelms the GSB and SE between 500 and 650 nm at timescales >0.5 ps and <20 ps. High-energy excitation also results in the slow induction (~200–300 ps) of an absorption feature characteristic of a triplet state (T_1) that persists beyond 1.2 ns, as evidenced with microsecond TAS (Fig. S2, ESI†). Notably, GSB can still be monitored at later time delays at probe wavelengths below 450 nm, even though this region overlaps with STA2.

We note that the data highlighted in Fig. 2(b) are somewhat different from what we reported previously for 420 nm excitation.²⁵ Fig. S3 (ESI†) presents the data for a solution of *cis*-4TCE that was exposed to air and ambient light for a period of 6 weeks. The exposed sample exhibits similarities with the previously published data, but not the data obtained with a fresh solution presented in Fig. 2(b). We therefore suspect the disparity between old and new samples is caused by a slow photooxidation of the sample over an extended period of time. A more detailed comparison of these data is discussed in the ESI†. Importantly, our new data facilitates better understanding of the mechanism and efficacy/efficiency for *cis*-to-*trans* switching.

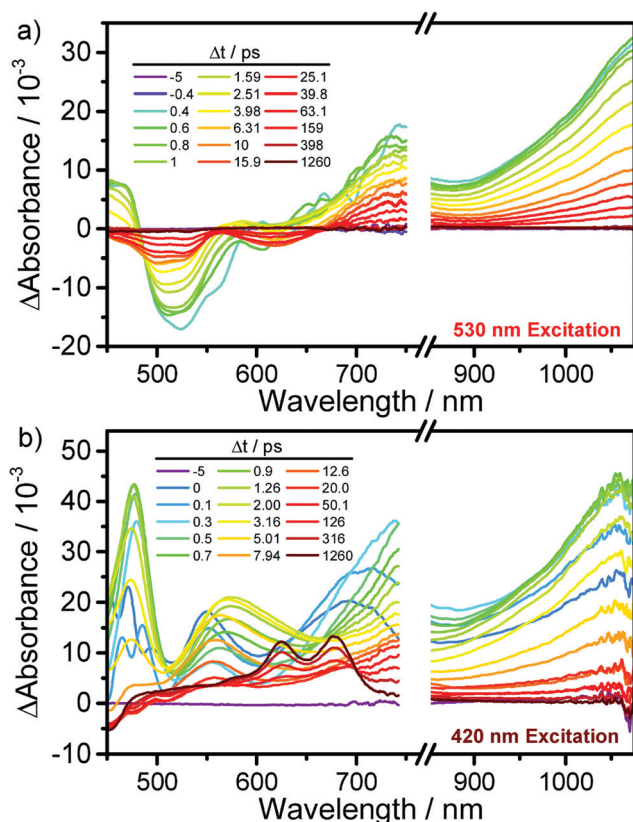


Fig. 2 Transient absorption spectra of *cis*-4TCE (**1**) (at representative time delays, Δt) collected with (a) low energy (530 nm) and (b) high energy (420 nm) excitation.

The TA spectral dynamics presented in Fig. 2 were analyzed using a global target principle component analysis (“global analysis”) in order to fit time-dependent spectral intensities collected at each wavelength to a multi-state relaxation between kinetically linked states or species with associated spectral components (“species associated spectra”, or SAS).^{32,33} Temporal fits used only data collected beyond 500 fs, as coherent artifacts observed around time zero in some spectral regions generated non-sensical SAS and generally resulted in poorer temporal fit quality; single-wavelength traces at key probe wavelengths are discussed further below for insights on the kinetics of signal induction and fast processes (<500 fs). In order to compare magnitudes and shapes of each SAS with variation in excitation wavelength, all data sets were normalized at their peak intensity (~745–750 nm) at a delay of 1 ps prior to global analysis (results are plotted as “Normalized Differential Absorption” or “Norm. Differential Abs.”). We found that all data sets collected with lower excitation energies were well-fit using a five-species/component sequential kinetic scheme (*i.e.* $A \rightarrow B \rightarrow C \rightarrow D \rightarrow E$). We also tested four- and six-component models: in all cases, four component models consistently resulted in poorer fit quality with systematic (time-dependent) residuals. A six component scheme provides no substantial improvement at low excitation energies (530 nm), but eliminated a small systematic discrepancy in the GSB region when fitting data collected at high excitation energy (420 nm) as described below.

Fig. 3 presents SAS (top) and transient cuts at various probe wavelengths together with their global fits (bottom) for data collected with the 530 nm excitation of *cis*-4TCE. The global spectral fit and fit residuals are presented in Fig. S4 (ESI†). Based on the results of the global fit, we characterize the spectral dynamics *vis-à-vis* the sequential kinetic scheme as follows: the first SAS exhibits signatures associated with GSB, SE, STA2, STA1, and STA0. The second SAS grows in on a 0.72 ps timescale and is associated with the appearance of STA3. STA1, STA0, and STA2 are slightly diminished in intensity in the second SAS whereas GSB and SE are reduced significantly in magnitude, suggesting that the appearance of STA3 “fills in” these features. SAS 2 decays with a lifetime of 2.6 ps; the third SAS has a lifetime that is only slightly longer (4.4 ps) and therefore appears to capture a peak shift in the region of STA3. The fourth SAS exhibits signatures of GSB, SE, STA1 and STA0, all of which decay to baseline (the fifth SAS) on a timescale of 32.4 ps. Notably, a four-state kinetic model lacks the third SAS obtained from the 5-state model, with poorer fit quality between 500 and 600 nm.

Similarly, Fig. 4 presents SAS (top) and transient cuts at various probe wavelengths together with their global fits (bottom) for data collected with 420 nm excitation of *cis*-4TCE. The global spectral fit and fit residuals are presented in Fig. S5 (ESI†). The SAS obtained from this fit have many similarities to those obtained at 530 nm: notably, the first, second and third SAS and the timescales for relaxation between them are similar for both excitation wavelengths (0.75 ps, 2.4, 4.5 ps). However, the peak absorption in the range of 500–600 nm is much larger for the second and third SAS with 420 nm *vs.* 530 nm excitation.

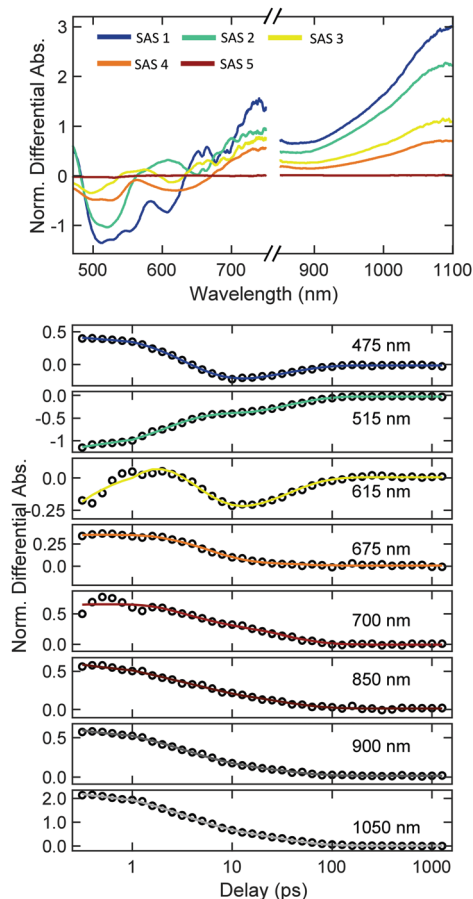


Fig. 3 Global fitting results for TAS data collected with 530 nm excitation of *cis*-4TCE. (top) Species-associated spectra (SAS) for five-component sequential kinetic model. (bottom) Time-dependent fits to transients at representative probe wavelengths. TAS data was normalized at 750 nm prior to global analysis to facilitate comparisons between SAS and temporal cuts for different excitation wavelengths.

The fourth and fifth SAS exhibit weak absorption across the visible with GSB below 500 nm; the conversion between these SAS is necessary to capture a partial GSB recovery on a 35.5 ps timescale, which is similar to the GSB recovery timescales obtained from fitting data collected at lower excitation energies. However, the final (sixth) SAS reflects the appearance of the structured absorption of the triplet, which is not seen at lower excitation energies and grows in on a timescale of 237 ps.

We also collected TAS data (probing only in the visible) following excitation at 565, 520, 510, 500, 490, 480, 475, 470, 460, and 440 nm. These data, along with outputs from their global analyses are presented in Fig. S6–S27 (ESI†). Lifetimes obtained from global fits of all TAS data are collected in Table 1. In summary, data collected at redder excitation wavelengths (<475 nm) were highly similar to the visible TAS shown in Fig. 2(a), yielding similar relaxation timescales and SAS from global spectral analyses. Data collected at bluer excitation wavelengths (>475 nm) exhibit signatures of triplet absorption at the latest delays probed (1 ns, SAS 6) as well as an increase in the magnitude of SAS 2 and SAS 3. The first four lifetimes obtained from global analysis (*i.e.* all but the ~200–300 ps

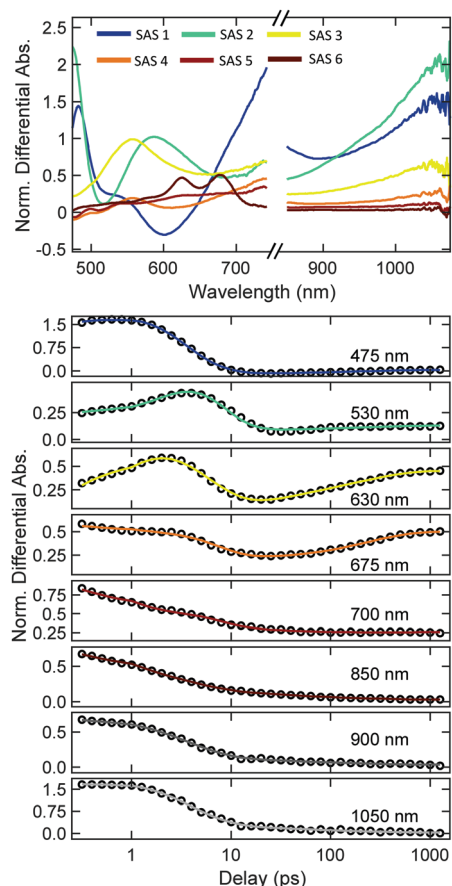


Fig. 4 Global fitting results for TAS data collected with 420 nm excitation of *cis*-4TCE. (top) Species-associated spectra (SAS) for six-component sequential kinetic model. (bottom) Time-dependent fits to transients at representative probe wavelengths. TAS data was normalized at 740 nm prior to global analysis to facilitate comparisons between SAS and temporal cuts for different excitation wavelengths.

timescale for triplet population at high excitation energies) are plotted in Fig. S28 (ESI†) against excitation wavelength. Although there is some scatter in the values with wavelength, these plots highlight that each lifetime is highly similar across excitation wavelength. Hence, the wavelength dependence of the observed spectral evolution is more strongly related to the relative magnitude of various spectral features and the appearance of the triplet at higher excitation energies.

In an effort to isolate the energetic onsets associated with the increased contribution of STA3 and the appearance of the triplet absorption, we have compared TA spectra collected at both 1 and 500 ps as a function of excitation wavelength across the visible. Fig. 5(a) compares spectra probed between 500 and 800 nm collected for each of the excitation wavelengths in the range 530–420 nm, 1 ps after excitation; these spectra have been normalized according to the peak absorbance of STA1 (750 nm) in order to highlight the intensity dependence for the remaining spectral features with excitation energy. It is obvious that there is a gradual increase in STA3 as a function of energy across the visible (similar to what is observed from relative magnitudes of SAS 2 and SAS 3 with excitation wavelength).

Table 1 Lifetimes of component species obtained from global analysis of TAS data with sequential kinetic models (i.e. $A \rightarrow B \rightarrow \text{etc.}$; # of lifetimes = # of states – 1)

	Excitation λ (nm)	Species lifetimes (ps)				
		τ_1	τ_2	τ_3	τ_4	τ_5
<i>cis</i> -4TCE (1)	565	0.4 ^a	2.3	5.0	45.9	—
	530	0.72	2.6	4.4	32.4	—
	520	0.48	3.8	3.8	38.6	—
	510	0.98	3.6	7.7	36.9	—
	500	0.50	3.7	3.7	41.0	—
	490	0.42	3.6	3.6	39.1	—
	485	0.45	3.3	4.4	39.9	—
	480	0.56	3.4	3.4	46.1	—
	475 (5 component)	0.59	4.0	4.0	41.0	—
	475 (6 component)	0.56	3.9	3.9	31.7	300 ^a
	470 (5 component)	0.57	3.4	3.4	49.0	—
	470 (6 component)	0.49	3.0	3.0	39.0	300 ^a
	460	0.86	3.9	3.9	31.3	288
	440	0.44	2.6	2.6	50 ^a	300 ^a
2 (<i>trans</i>)	420	0.75	2.4	4.5	35.5	237
	530	0.5 ^a	1.5 ^a	8.2	57.6	—
2 (<i>cis</i>)	420	0.5 ^a	1.5	9.5	62.0	—
	530	0.40	3.5	3.5	61.8	—
3	420	1.1	2.6	7.6	77.4	—
	490	4.6	321	—	—	—

^a Lifetime constrained.

In order to isolate the relative contribution of STA3 as a function of excitation wavelength, the spectrum at 1 ps collected with 530 nm excitation was subtracted from spectra collected with shorter excitation wavelengths at the same time delay, producing the contour plot shown in Fig. 5(b). Performing this subtraction serves to remove contributions from STA1, GSB, and SE leaving only STA3. STA3 already appears with 530 nm excitation, however as can be seen in the subtracted plot, the contribution of STA3 increases gradually from 530 to 490 nm and then significantly with excitation energy at ~ 470 nm, indicating the presence of at least two energetic thresholds for the appearance of this feature. Fig. 6 plots the relative intensity (determined by integration between 525 and 575 nm) of the post-subtracted STA3 feature together with the steady-state absorption spectrum of *cis*-4TCE.

Similarly, Fig. 5(c) plots the dependence with excitation wavelength of the intensity of the T_1 absorption observed at 500 ps. These data were combined by normalizing each TAS data set with respect to the STA1 signal at 1 ps, but no signal subtractions were necessary to isolate features of the triplet absorption as there are no overlapping spectral features at this delay. The onset for triplet state population can be seen clearly as the excitation energy approaches ~ 470 nm, closely aligning with an appreciable increase in STA3. Fig. 6 plots the relative triplet absorption intensity (integrated between 600 and 700 nm) against the absorption spectrum of *cis*-4TCE.

Coherent artifacts near time zero in some spectral regions make it difficult to fit spectral dynamics at the earliest delays *via* global analysis. In order to get a better handle on signal induction and evolution on sub-ps timescales, we fit transient cuts at wavelengths corresponding to specific spectral features using multiexponential functions convoluted with the instrument

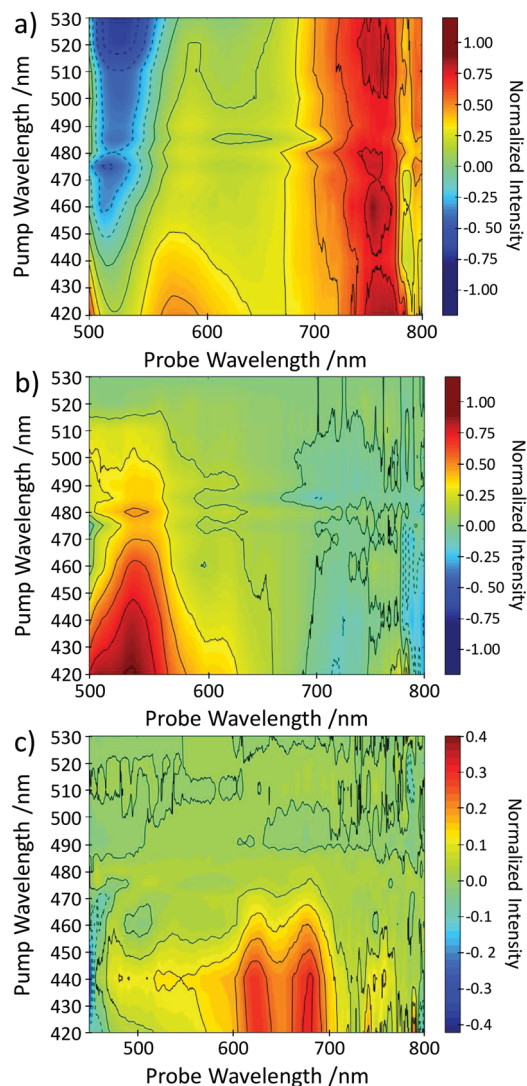


Fig. 5 Excitation wavelength-dependence of 4TCE TA spectral features. (a) Excitation wavelength-dependence of TA spectra collected with a 1 ps pump–probe delay (normalized at ~ 750 nm). (b) Wavelength dependent difference spectra at 1 ps delay obtained by subtracting the normalized TA spectrum collected at 530 nm excitation to highlight excitation dependence of the 530 nm transient absorption feature ("STA3"). (c) Wavelength dependent spectra collected 500 ps following excitation to highlight onset for the appearance of T_1 absorption.

response (Fig. S29, S30 and Table S1, ESI[†]). For data collected with 530 nm excitation, STA0 (probed at 1050 nm) appears at the instrument limit and only decays on picosecond or longer timescales. In contrast STA1 (probed at 750 nm) decays by $\sim 52\%$ whereas STA2 (probed at 460 nm) grows in on comparable ultrafast timescales outside of the instrument resolution (0.29 vs. 0.2). This leads us to believe that an ultrafast structural relaxation in the excited state may involve a rise in STA2 at the expense of transition strength for STA1. In contrast, when *cis*-4TCE is excited at 420 nm all features (STA0, STA1 and STA2) appear with a 0.3 ps induction outside of the instrument response, suggesting that the spectral dynamics captured by TAS follow an ultrafast relaxation to S_1 from a dark excited state of *cis*-4TCE.

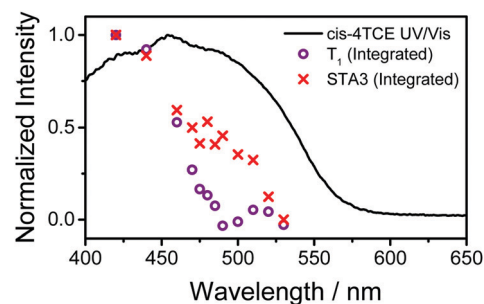


Fig. 6 Relative intensities of TA spectral features (integrated 525–575 nm for STA3, 600–700 nm for T_1 absorption) observed for 4TCE with excitation wavelength compared to the *cis*-4TCE absorption spectrum. Traces/spectra are normalized to their peak intensities.

Finally, we conducted additional measurements with analogs of 4TCE to explore structure-dynamics relationships that underlie 4TCE photophysics. The 4TCE derivative 2, which is brominated on the α Cs (relative to S) of the terminal thienyl rings, was studied to investigate mechanical influences on electronic deactivation pathways. Our hypothesis is that the positioning of the bromine atoms at the periphery of switch structure introduces massive substituents that would modify timescales associated with large-scale geometry changes. We also recognize that Br could increase the rate of ISC observed with higher excitation energies due to larger spin–orbit coupling (*i.e.* heavy-atom effect). Fig. S31–S38 (ESI[†]) shows TA spectra collected with excitation of both isomers of 4TCE-Br at both 530 nm and 420 nm as well as their global fitting results; species lifetimes obtained from global fits are reported in Table 1.

The spectral evolution observed for each isomer at each excitation wavelength is qualitatively similar to that observed for unsubstituted 4TCE; only differences in some relaxation lifetimes are noteworthy. Notably, the *trans* isomer of the brominated structure deactivates more slowly (~ 60 ps S_1 lifetime) than unbrominated *trans*-4TCE (40 ps),²⁵ consistent with the large scale structural dynamics associated with *trans*-to-*cis* isomerization (a faster relaxation timescale of ~ 8 ps is largely unchanged with bromination, Table 1). Similarly, the longest relaxation timescale observed following 530 nm excitation of *cis* 4TCE is significantly dilated upon bromination, ~ 30 –40 ps vs. 64 ps. Global fitting of data collected with 420 nm excitation reveals that the triplet appears on a 73 ps timescale; this is quite similar to the GSB recovery timescale for *cis*-2 determined for 530 nm excitation, and the six-component kinetic scheme does not resolve distinctly the GSB recovery and triplet appearance timescales observed for the 420 nm excitation of *cis*-4TCE. The somewhat faster triplet appearance suggests stronger spin–orbit coupling and a faster ISC rate for the brominated analog.

In contrast, 3 was studied to examine the impact of structurally constraining the ethene bridge on photochemical dynamics. Transient spectra collected with 3 exhibit features similar to STA0, STA1, STA2 and SE. Waterfall plots of these spectra are shown in Fig. 7. All the features present in the transient spectra were analyzed by global analysis (3 components) to determine the best overall fits; SAS and time-dependent cuts at representative

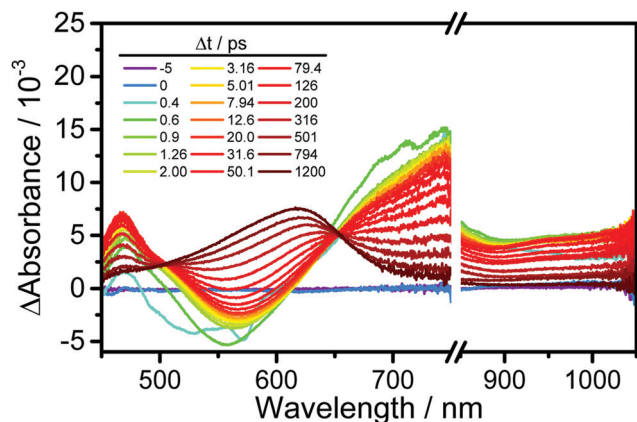


Fig. 7 Transient spectra for **3** collected with 490 nm excitation.

probe wavelengths are shown in Fig. 8, with the global fit and residuals plotted in Fig. S39 (ESI†). The first and second SAS exhibit lifetimes of 4.6 ps and 321 ps, leaving behind a broad absorption feature in the visible (SAS 3) that closely matches the position of triplet absorption for 4TCE and related

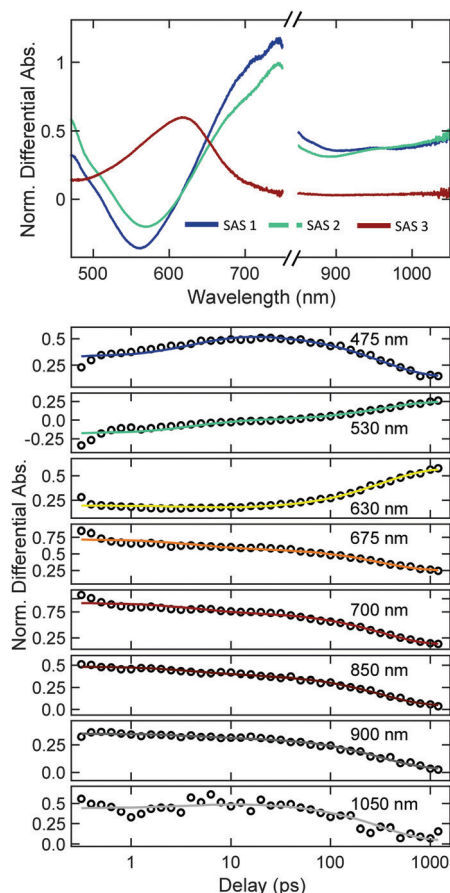


Fig. 8 Global fitting results for TAS data collected with 490 nm excitation of **3**. (top) Species-associated spectra (SAS) for a three-component sequential kinetic model. (bottom) Time-dependent fits to transients at representative probe wavelengths. Data was normalized to intensity at 725 nm at 1 ps before global fitting.

oligothiophenes. The 4.6 ps timescale, associated largely with the growth of STA2 (*i.e.* absorption below 500 nm), most likely corresponds with an excited-state nuclear relaxation. In contrast the 321 ps relaxation with associated isosbestic points is consistent with nonradiative decay dominated by intersystem crossing as indicated by the appearance of an intense triplet absorption spectrum. This data reveals that slow triplet population for a structure like 4TCE could be relatively efficient on a 200–300 ps timescale if constraints are introduced that impede nuclear dynamics that facilitate fast nonradiative decay. Furthermore, like 4TCE, **3** does not show any evidence of photocyclization. Below we draw comparisons between the photophysics of these compounds to understand photoresponses of 4TCE and how they depend on its structural properties.

Discussion

The transient spectral data presented above and in our previous investigations portend rich multistate photophysical dynamics for *cis*-4TCE. These data suggest specifically that the low quantum yield for *cis* to *trans* isomerization likely originates from a combination of a thermal distribution of conformers including both reactive and nonreactive structures as well as a complex photoinduced non-radiative relaxation cascade to the triplet state that is the gateway for isomerization for a reactive conformer. We consider each of these contributing factors below to build a reasonable kinetic model for the photoresponses of *cis*-4TCE and to assess losses to its switching efficiency.

Photoresponses of molecular conformers of *cis*-4TCE

Fig. 2(a) and 3 reveal a complex spectral evolution following low-energy excitation of 4TCE at 530 nm: a large initial GSB rapidly disappears as STA3 grows in, but is clearly diminished even after STA3 disappears; the remaining GSB (about 25% of the initial bleach) then recovers on a ~ 40 ps timescale. In total, this reflects a superposition of two spectral dynamics with GSB recovery occurring on distinct timescales that could be explained in one of two ways: (1) pathway branching from the Franck-Condon region of a photoprepared molecular excited state or (2) the presence of two or more molecular conformers with different relaxation dynamics. The former is attributed, for example, with the *E/Z* vs. electrocyclization dynamics of *cis*-stilbene and related compounds.^{34–38} Contributions from multiple conformers in the photoresponses of molecular photo-switches has precedent as well: for example, fluorinated stilbenes have been shown to have rotamer-dependent relaxation kinetics.³⁹ Also, as described above, multiple conformations of dithienylethenes are well-known,^{18,19} where the so-called “antiparallel” conformer (*i.e.* pendant thiophene rings aligned mutually antiparallel) is critical for photocyclization.

A conformer distribution at room temperature seems much more likely of these two explanations for the multipatterned spectral dynamics seen here given the structural similarity between *cis*-4TCE and related diarylethenes. We note that we were unable to isolate signatures of a conformer distribution

using low-temperature NMR, which suggests that the energetic barrier for fluctuations between structures is likely quite low and that these fluctuations are relatively rapid. We have therefore explored relevant structural conformers with a set of geometry optimization calculations. Fig. 9 shows the geometries associated with three conformers of *cis*-4TCE calculated using TD-DFT at the TD-M052X level of theory and a 6-31g* basis set; their corresponding calculated absorption spectra are plotted in Fig. S40 (ESI†). Two conformers with roughly parallel orientation of the thienyl rings on either side of the ethene bond, henceforth termed P_A and P_B , are similar to the structure obtained by X-ray crystallography that was published previously.²⁴ Structurally, P_A and P_B differ according to the orientation of one of the bithienyl ‘arms’ with minimum energies separated energetically by only 33.8 cm⁻¹. In contrast, the ‘anti-parallel’ (AP) conformer, the structure that would be predicted to facilitate photocyclization, lies approximately 450 cm⁻¹ higher than P_A . While the P and AP classification we use here is based on conformer terminology applied to photocyclizable diarylethenes, we can also classify these structures according to the relative orientation of the CN dipoles and those of the nearest thienyl groups: in the AP structure these local dipoles are oriented parallel to one another, resulting in a large net molecular dipole; in contrast, these are oriented roughly antiparallel to one another in the P_A and P_B conformers, subject to mutual repulsive interactions between the S sites that prohibit a true antiparallel orientation, and result in a net reduction of the molecular dipole.

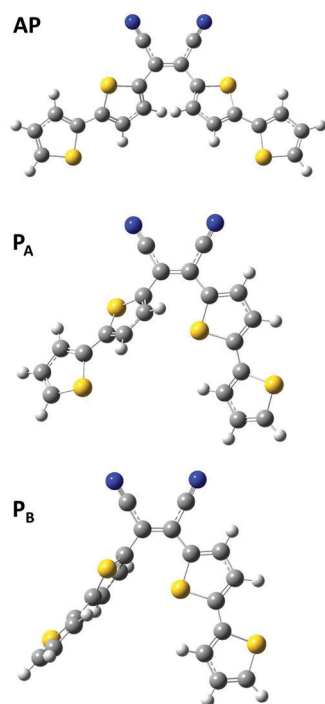


Fig. 9 Molecular geometries calculated at the M052X level of theory utilizing a 6-31g* basis set. The two parallel structures, P_A and P_B , are energetically separated by only 33.8 cm⁻¹. The ‘anti-parallel’ (AP) conformer lies approximately 450 cm⁻¹ higher than P_A .

Based on computed energetics, these three structures are predicted to be present in a ratio of 51:43:6 ($P_A:P_B:AP$) at room temperature. Such a distribution, alongside the heavily overlapped ground-state absorption transitions of these conformers (Fig. S40, ESI†), means that the multicomponent spectral dynamics we observe can be ascribed to the presence of different conformers that are excited simultaneously. We therefore can attribute portions of the observed excited-state spectral dynamics and their excitation wavelength dependence to specific conformers, starting with the biphasic GSB recovery. The GSB recovers on fast (<10 ps) vs. slow (~40 ps) timescales in a roughly 2.9:1 proportion for excitation at wavelengths > 460 nm – that is, the total initial GSB (at 0.6 ps) is 3.9 times larger than the GSB observed after fast processes are complete (at 8 ps), as demonstrated in Fig. S41 (ESI†). Although our calculations predict that P_A and P_B should appear in roughly equal proportions ($P_A/P_B \sim 1.2$), the oscillator strengths computed for their lowest-energy absorption transitions differ by a factor of ~2.3 (f_{P_A}/f_{P_B}). Thus, we could predict that P_A and P_B are excited at a ratio of 2.76:1 in the visible, which is close to the partitioning between fast and slow GSB recovery observed experimentally. We therefore attribute the faster spectral dynamics and GSB recovery to deactivation of the excited P_A *cis*-4TCE conformer and the slower (~40 ps and longer) dynamics and GSB recovery to deactivation of the excited P_B *cis*-4TCE conformer. We note that although we used a sequential kinetic model for our global spectral analyses, this correspondence with photophysics of two separate structures is reasonable given the large separation in timescales for fast and slow dynamics.

The relaxation of these conformers following direct excitation to S_1 at visible wavelengths (e.g. 530 nm) are summarized with the Jablonski diagram presented in Fig. 10. While it would not be possible to separate any fast spectral shifting associated with e.g. vibrational relaxation of P_B from the electronic relaxation dynamics of P_A via global analysis if these occur on similar timescales, the appearance and decay of STA3 is clearly correlated with a sizeable and fast GSB recovery. Hence, we ascribe the appearance of the transient absorption feature STA3 with the population of an intermediate state that facilitates relaxation of P_A between S_1 and S_0 . This could either be an intermediate electronic state, S_n , or an S_1 geometry (S_1') with improved coupling to the S_0 surface for this conformer; the

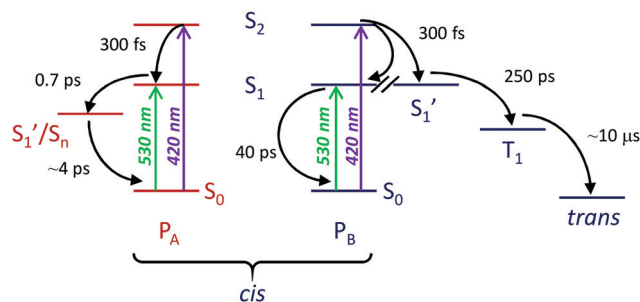


Fig. 10 Jablonski diagram of energy- and conformer-dependent photophysics of *cis*-4TCE.

latter seems sensible given that SAS 2 shares many of the same spectral features as SAS 1 (e.g. STA0 and STA1, Fig. 3 and 4). We expect that an intermediate state is responsible for the faster deactivation of P_A vs. P_B *cis*-4TCE. In contrast, the slower deactivation of P_B occurs through a direct internal conversion between S_1 and S_0 , which could be gap-law limited.

Only a small population of the AP conformer is predicted computationally, but the lowest-energy transition of this conformer is computed to fall to longer wavelength (~ 550 nm vs. ~ 500 nm) and to have a significantly larger oscillator strength than both P_A and P_B (0.845 vs. 0.509 and 0.220). Thus, we might expect to see signatures in our TAS data associated with excitation of the AP conformer at the longest excitation wavelengths used. However, TA spectral dynamics observed with 565 nm excitation do not reveal any additional timescales or spectral features beyond what is seen at higher energies. This leads us to believe that either the AP conformer is much higher in energy relative to P_A and P_B than computed, that there is an appreciable activation barrier between the AP and P conformers in the ground state, or that the *trans*-to-*cis* photochemistry used to prepare the sample for our experiments is biased towards population of the P conformers. Importantly, the apparent lack of a thermal AP conformer population implies that electrocyclization is not a viable deactivation pathway for this switch.

Energy-dependence of 4TCE photophysics and photochemistry

While transient data collected with low-energy excitation provides evidence for the presence of more than one *cis*-4TCE conformer based on a multicomponent spectral evolution, energy-dependence of spectral dynamics provides evidence for cascading photophysical pathways that are critical to driving its photoswitching mechanism. In order to assign a coherent excited-state relaxation mechanism to the spectral evolution captured in Fig. 2(b) it is important to determine whether the relaxation of only one or both conformers is affected by excitation energy. We first note that global analysis results reveal no significant changes in the lifetimes or the shapes of species associated spectra (only their intensities) for the fastest spectral dynamics observed in TAS data collected with excitation across 530–420 nm. Based on our assignment of fast spectral evolution to the photoresponse of the P_A conformer, we posit that there are no significant changes in the deactivation mechanism of this conformer with excitation energy. In contrast, the contribution of the slower (~ 40 ps) GSB recovery (i.e. relaxation between SAS 4 to SAS 5) observed at lower excitation energies (> 475 nm) that we ascribe to deactivation of the P_B conformer decreases at higher energies (< 475 nm) where we also see the slow growth of triplet population on a ~ 240 ps timescale (SAS 6). As isomerization occurs from the lowest triplet, only the P_B conformer (what we henceforth call the “reactive conformer”) is ultimately responsible for photoswitching of *cis*-4TCE at higher excitation energies.

As GSB recovery at lower excitation energies occurs significantly faster than the slow appearance of the triplet (~ 40 vs. ~ 240 ps), the latter must require the preparation of an S_1 structure that is stable against the faster internal conversion back to the ground state. This expectation is consistent with

our observations of efficient triplet population in the structurally constrained compound 3 which is stable against rapid IC and exhibits a 321 ps S_1 lifetime. As the energetic onset for triplet appearance is abrupt rather than gradual for *cis*-4TCE (Fig. 6), it seems unlikely that this is achieved *via* direct excitation to the Franck–Condon region of the S_1 surface. Rather, we note that our computational spectra (Fig. S40, ESI†) show that the S_2 electronic state (second optically accessible, primarily HOMO–1 to LUMO in character) lies ~ 0.5 eV above the lowest-energy transition (HOMO to LUMO) near the energetic onset for triplet population, and that a transition to this state has appreciable oscillator strength for the P_B conformer.²⁵ Given that all excited-state absorption features grow in with a 300 fs induction at higher excitation energies (Fig. S30 and Table S1, ESI†), it is most sensible to ascribe the preparation of a metastable, longer-lived S_1 configuration (S_1') to a non-adiabatic relaxation following direct excitation to a higher-lying electronic surface.

This mechanism is consistent with the difference in shape of SAS 4 and SAS 5 (Fig. 4): SAS 4 exhibits the S_1 TA spectral features GSB, SE and STA1 that are observed at lower excitation energies and that are presumably characteristics of the S_1 Franck–Condon region for emission and the region from which IC occurs with a ~ 40 ps lifetime. In contrast, SAS 5 only exhibits GSB and STA1; the conspicuous lack of the SE signal is consistent with an excited-state geometry distinct from the minimum energy S_1 geometry reached at low excitation energies. Hence, the gateway to reaching the triplet manifold (and therefore *cis* to *trans* isomerization) appears to involve excitation to S_2 followed by a branching between IC-active and ISC-active S_1 geometries as a result of $S_2 \rightarrow S_1$ relaxation. We estimate a branching ratio of 50% based on the drop of STA1 and STA0 between SAS 4 and SAS 5 for excitation wavelengths < 470 nm. This proposed mechanism for triplet population (and hence isomerization) is summarized on the right half of Fig. 10.

Fig. 5 and 6 reveal sharp onsets to both the triplet and STA3 absorption features as the excitation is tuned to higher energies. The magnitude of STA3 increases gradually with excitation energy when pumped directly to S_1 (565–475 nm), but dramatically as S_2 becomes accessible (< 475 nm). Notably the $S_0 \rightarrow S_2$ transitions for both P_A and P_B are computed to occur at similar wavelengths (Fig. S40, ESI†), which could explain why STA3 and T_1 absorption intensities both increase markedly at excitation wavelengths below 470 nm. Based on global analysis results, it appears that deactivation of S_2 P_A *cis*-4TCE does not alter the timescales of dynamics on the S_1 surface, but does increase the magnitude of STA3 with excitation energy. These behaviors suggest that the relative fraction of P_A vs. P_B excited increases somewhat at higher energies. Although we cannot reconcile this with our computed conformer spectra, it is consistent with the trend in fast vs. slow GSB recovery amplitudes with excitation wavelength determined from data collected with longer excitation wavelengths (Fig. S41, ESI†).

Photoswitch efficiency

Our analysis of the conformer- and energy-dependent relaxation dynamics of photoexcited *cis*-4TCE allows us to assess

quantitative limitations to its *cis*-to-*trans* photoswitching efficiency. The presence of at least two *cis*-4TCE conformers at room temperature with characteristically different energy-dependent deactivation kinetics immediately reveals a fundamental photo-switch inefficiency: given the $\sim 2.9:1$ ratio of GSB recovery associated with the P_A and P_B conformers, and the observation that the fast deactivation of the P_A conformer to its ground state is unchanged with excitation energy and therefore that P_A is a nonreactive/nonswitchable conformer, we identify that a large fraction of absorbed photons ($>75\%$) are not available to excite the reactive P_B conformer. This situation is analogous to the inefficiency of parallel conformers for the electrocyclization of related dithienylethenes. This fraction appears to increase with increasing excitation energy, as evident by increasing dominance of TA features ascribed to conformer P_A (e.g. Fig. S41, ESI†). Although a GSB analysis is not possible at higher excitation energies (e.g. 420 nm) where STA3 and triplet absorption strongly overlap the bleach, we can approximate that 85% of incident photons at 420 nm are absorbed by nonreactive P_A based on the relative intensity of STA0 before and after fast signal decay (e.g. 0.5 vs. 12.6 ps, 6.7:1).

As we estimate $\sim 50\%$ branching between IC-active S_1 and ISC-active S_1' configurations of P_B following $S_2 \rightarrow S_1$ relaxation, we conclude that there is a ~ 7.5 – 12.5% yield for preparing the ISC-active S_1' geometry of P_B *cis*-4TCE in an ensemble of conformers. As only spectral signatures of the triplet persist on timescales of 1 ns, we presume that most of the initial *cis*-4TCE excited-state population is lost through competing non-radiative relaxation to the ground-state, which we are unable to monitor directly *via* GSB recovery due to the spectral overlap of these features. We previously determined the *cis*-to-*trans* switching quantum yield at 420 nm through actinometry as $\sim 5\%$. Our previous work also revealed that the two isomers likely have a common minimum energy triplet geometry. Experimentally, triplet sensitization of the *trans* isomer does not induce isomerization, whereas sensitization of the *cis* isomer does, suggesting to us that isomerization of the *cis* triplet likely occurs with near unit efficiency. Therefore we estimate an upper limit to the ISC quantum yield of ~ 0.4 – 0.67 for P_B S_1' , with a corresponding ISC rate constant of ~ 1.6 – $2.7 \times 10^9 \text{ s}^{-1}$. This is in reasonable when compared to ISC yields and rates observed for oligothiophenes of comparable length^{40,41} (e.g. α -pentathiophene $QY_{ISC} = 0.59$, and $k_{ISC} = 0.72, 1.7$ and $5.9 \times 10^9 \text{ s}^{-1}$ for ter-, quater- and pentathiophene, respectively⁴²). Relatedly we find that the fluorescence quantum yield of **3** is 0.049 ± 0.002 (Fig. S42, ESI†), implying a significant nonradiative deactivation rate; as ISC must be competitive with IC in **3** in order to observe appreciable triplet absorption in our TAS measurements, Φ_{ISC} likely falls in the neighborhood of ~ 0.5 , comparable to our estimation for the ISC-active geometry S_1' P_B *cis*-4TCE.

Finally we return to the question of why a photocyclization mechanism is not accessible for *cis*-4TCE. Notably, **3** also does not exhibit evidence for photocyclization, although it has been shown previously that a structure analogous to **3** with only a single methylated α -thienyl group on either side of the

cyclopentene bridge can cyclize with UV photoexcitation.⁴³ This suggests that delocalization of S_1 in **3** inhibits localized bond formation. As the lowest electronic states of 4TCE exhibit either push-pull CT character or extended pi-delocalization, localized bond formation is likewise not possible. Importantly, our studies here reveal that a combination of multiple relaxation pathways is able to efficiently funnel any photoexcited population back to the ground state, or to the triplet state for *E/Z* isomerization in lower yield. While we cannot discount the possibility of photocyclization *via* excitation to higher lying excited states (excitation $< 420 \text{ nm}$), we anticipate that relaxation cascades similar to those seen at lower energies should outcompete cyclization in the deactivation of photoexcited *cis*-4TCE. Additionally, our analysis indicates that the AP conformer of *cis*-4TCE, which is likely a necessary geometry for cyclization, is not present in the *cis*-4TCE ensemble at room temperature, further inhibiting the possibility of this reaction pathway.

Conclusions

In summary, we have utilized a comprehensive study of the excitation-energy dependent photophysics of *cis*-4TCE in combination with TA studies of related structures to more deeply characterize the origins of this compound's photoisomerization response and to identify primary sources of its switching inefficiency. In analogy to photocyclizing diarylethene photo-switching, we have found that the photoresponses of 4TCE in solution is significantly impacted by the presence of two molecular conformers: a reactive conformer (P_B *cis*-4TCE) that exhibits slow IC at low excitation energies ($> 475 \text{ nm}$) but that isomerizes at high excitation energies ($< 475 \text{ nm}$); and a non-reactive conformer (P_A) that rapidly relaxes to its ground state at all excitation energies studied here *via* an intermediate state. The presence of a non-reactive conformer represents a significant quantum-yield loss (75–85%) for isomerization. Additionally, isomerization of the P_B conformer involves excitation of its S_2 state followed by an electronic relaxation cascade to an S_1 geometry (S_1') for which ISC is competitive with IC. Relaxation of this S_1 geometry ultimately populates the lowest triplet level that is the gateway to *cis*-to-*trans* photoisomerization of 4TCE with an ISC quantum yield of 0.4–0.67. Although we estimate that the triplet isomerization yield is likely quite significant (approaching unity), losses due to the presence of P_A and the relaxation cascade to the reactive triplet significantly lower the isomerization quantum yield (5%). These rapid relaxation cascades, CT character and pi-delocalization of the lowest electronic states of 4TCE, and a virtually nonexistent thermal population of a cyclizable conformer geometry (AP) effectively eliminate a competing photocyclization pathway.

Together, our findings directly explain the low quantum efficiency for *cis*-to-*trans* isomerization of 4TCE measured actinometrically, but also point to avenues for improving the switching response of this compound. For example, in analogy to efforts to improve the cyclization yields of diarylethenes,¹⁸ a structurally-modified 4TCE compound that eliminates presence of the

nonreactive conformer could increase the *cis-to-trans* isomerization quantum yield (with the potential to achieve a switch efficiency of as much as 30% for a pure P_B ensemble). This would enhance the *trans* concentration at the photostationary state and improve performance as a two-state switch. The efficiency of the switch could be improved more significantly by improving the yield of reactive triplet. This could perhaps be achieved through inclusion of heavier elements (*e.g.* using selenophene or tellurophene analogs of the thienyl pendant rings) to drastically increase spin-orbit coupling and ISC rates.⁴⁴ Alternatively this could possibly be achieved using a chemically linked triplet sensitizer. Through careful selection of the sensitizer, this scheme could also be used to manipulate or extend the wavelength range for light sensitization.¹² These are all directions we are continuing to explore to improve the performance of 4TCE and extend the palette of *E/Z* photoswitches.

Conflicts of interest

There are no conflicts of interest to declare.

Acknowledgements

Photophysical studies and synthesis of **3** were supported by NSF-CHE-1607821 (A. E. B. & J. D. T.). Photophysical studies were also supported in part by a JHU Catalyst Award (A. E. B.). Synthesis of 4TCE and its brominated derivative were supported by NSF-CHE-1465131 (T. L.).

References

- 1 A. Fihey, A. Perrier, W. R. Browne and D. Jacquemin, Multiphotochromic Molecular Systems, *Chem. Soc. Rev.*, 2015, **44**, 3719–3759.
- 2 M. Irie, Diarylethenes for Memories and Switches, *Chem. Rev.*, 2000, **100**, 1685–1716.
- 3 M. Irie, T. Fukaminato, K. Matsuda and S. Kobatake, Photochromism of Diarylethene Molecules and Crystals: Memories, Switches, and Actuators, *Chem. Rev.*, 2014, **114**, 12174–12277.
- 4 M. T. W. Milder, J. Areephong, B. L. Feringa, W. R. Browne and J. L. Herek, Photoswitchable Molecular Wires: From a Sexithiophene to Dithienylethene and Back, *Chem. Phys. Lett.*, 2009, **479**, 137–139.
- 5 D. Dulic, S. J. van der Molen, T. Kudernac, H. T. Jonkman, J. J. D. de Jong, T. N. Bowden, J. van Esch, B. L. Feringa and B. J. van Wees, One-Way Optoelectronic Switching of Photochromic Molecules on Gold, *Phys. Rev. Lett.*, 2003, **91**, 207402.
- 6 S. L. Gilat, S. H. Kawai and J.-M. Lehn, Light-Triggered Molecular Devices: Photochemical Switching of Optical and Electrochemical Properties in Molecular Wire Type Diarylethene Species, *Chem. – Eur. J.*, 1995, **1**, 275–284.
- 7 W. Szymanski, J. M. Beierle, H. A. V. Kistemaker, W. A. Velema and B. L. Feringa, Reversible Photocontrol of Biological Systems by the Incorporation of Molecular Photoswitches, *Chem. Rev.*, 2013, **113**, 6114–6178.
- 8 S. Gozem, F. Melaccio, H. L. Luk, S. Rinaldi and M. Olivucci, Learning from Photobiology how to Design Molecular Devices Using a Computer, *Chem. Soc. Rev.*, 2014, **43**, 4019–4036.
- 9 I. Tochitsky, M. A. Kienzler, E. Isacoff and R. H. Kramer, Restoring Vision to the Blind with Chemical Photoswitches, *Chem. Rev.*, 2018, **118**, 10748–10773.
- 10 B. L. Feringa, The Art of Building Small: From Molecular Switches to Molecular Motors, *J. Org. Chem.*, 2007, **72**, 6635–6652.
- 11 F. Terao, M. Morimoto and M. Irie, Light-Driven Molecular-Crystal Actuators: Rapid and Reversible Bending of Rodlike Mixed Crystals of Diarylethene Derivatives, *Angew. Chem.*, 2012, **51**, 901–904.
- 12 S. Fredrich, R. Göstl, M. Herder, L. Grubert and S. Hecht, Switching Diarylethenes Reliably in Both Directions with Visible Light, *Angew. Chem., Int. Ed.*, 2016, **55**, 1208–1212.
- 13 M. M. Lerch, M. J. Hansen, W. A. Velema, W. Szymanski and B. L. Feringa, Orthogonal Photoswitching in a Multifunctional Molecular System, *Nat. Commun.*, 2016, **7**, 12054.
- 14 M. Herder, B. M. Schmidt, L. Grubert, M. Patzel, J. Schwarz and S. Hecht, Improving the Fatigue Resistance of Diarylethene Switches, *J. Am. Chem. Soc.*, 2015, **137**, 2738–2747.
- 15 A. D. Dunkelberger, R. D. Kieda, J. Y. Shin, R. R. Paccani, S. Fusi, M. Olivucci and F. F. Crim, Photoisomerization and Relaxation Dynamics of a Structurally Modified Biomimetic Photoswitch, *J. Phys. Chem. A*, 2012, **116**, 3527–3533.
- 16 M. Boggio-Pasqua, M. Ravaglia, M. J. Bearpark, M. Garavelli and M. A. Robb, Can Diarylethene Photochromism Be Explained by a Reaction Path Alone? A CASSCF Study with Model MMVB Dynamics, *J. Phys. Chem. A*, 2003, **107**, 11139–11152.
- 17 C. L. Ward and C. G. Elles, Cycloreversion Dynamics of a Photochromic Molecular Switch via One-Photon and Sequential Two-Photon Excitation, *J. Phys. Chem. A*, 2014, **118**, 10011–10019.
- 18 S. Aloïse, M. Sliwa, Z. Pawlowska, J. Réhault, J. Dubois, O. Poizat, G. Buntinx, A. Perrier, F. Maurel, S. Yamaguchi and M. Takeshita, Bridged Photochromic Diarylethenes Investigated by Ultrafast Absorption Spectroscopy: Evidence for Two Distinct Photocyclization Pathways, *J. Am. Chem. Soc.*, 2010, **132**, 7379–7390.
- 19 Y. Ishibashi, M. Fujiwara, T. Umesato, H. Saito, S. Kobatake, M. Irie and H. Miyasaka, Cyclization Reaction Dynamics of a Photochromic Diarylethene Derivative as Revealed by Femtosecond to Microsecond Time-Resolved Spectroscopy, *J. Phys. Chem. C*, 2011, **115**, 4265–4272.
- 20 R. B. Woodward and R. Hoffmann, The Conservation of Orbital Symmetry, *Angew. Chem., Int. Ed. Engl.*, 1969, **8**, 781–853.
- 21 C. Bertarelli, M. C. Gallazzi, F. Stellaci, G. Zerbi, S. Stagira, M. Nisoli and S. De Silvestri, Ultrafast Photoinduced Ring-Closure Dynamics of a Diarylethene Polymer, *Chem. Phys. Lett.*, 2002, **359**, 278–282.
- 22 A. A. Beharrya and G. A. Woolley, Azobenzene Photoswitches for Biomolecules, *Chem. Soc. Rev.*, 2011, **40**, 4422–4437.
- 23 P. D. Wildes, J. G. Pacifici, G. Irick Jr. and D. G. Whitten, Solvent and Substituent Effects on the Thermal Isomerization of Substituted Azobenzenes. A Flash Spectroscopic Study, *J. Am. Chem. Soc.*, 1971, **93**, 2004–2008.

- 24 X. Guo, J. Zhou, M. A. Siegler, A. E. Bragg and H. E. Katz, Visible-Light Triggered Molecular Photoswitch Based on Reversible *E/Z* Isomerization of a 1,2 Dicyanoethene Derivative, *Angew. Chem., Int. Ed.*, 2015, **54**, 4782–4786.
- 25 J. Zhou, X. Guo, H. E. Katz and A. E. Bragg, Molecular Switching via Multiplicity-Exclusive *E/Z* Photoisomerization Pathways, *J. Am. Chem. Soc.*, 2015, **137**, 10841–10850.
- 26 M. S. Molloy, J. A. Snyder and A. E. Bragg, Structural and Solvent Control of Nonadiabatic Photochemical Bond Formation: Photocyclization of *O*-Terphenyl in Solution, *J. Phys. Chem. A*, 2014, **118**, 3913–3925.
- 27 W. Yu, T. J. Magnanelli, J. Zhou and A. E. Bragg, Structural Heterogeneity in the Localized Excited States of Poly(3-hexylthiophene), *J. Phys. Chem. B*, 2016, **120**, 5093–5102.
- 28 M. J. Frisch, G. W. Trucks, H. B. Schlegel, G. E. Scuseria, M. A. Robb, J. R. Cheeseman, G. Scalmani, V. Barone, B. Mennucci, G. A. Petersson, H. Nakatsuji, M. Caricato, X. Li, H. P. Hratchian, A. F. Izmaylov, J. Bloino, G. Zheng, J. L. Sonnenberg, M. Hada, M. Ehara, K. Toyota, R. Fukuda, J. Hasegawa, M. Ishida, T. Nakajima, Y. Honda, O. Kitao, H. Nakai, T. Vreven, J. A. Montgomery, Jr., J. E. Peralta, F. Ogliaro, M. Bearpark, J. J. Heyd, E. Brothers, K. N. Kudin, V. N. Staroverov, R. Kobayashi, J. Normand, K. Raghavachari, A. Rendell, J. C. Burant, S. S. Iyengar, J. Tomasi, M. Cossi, N. Rega, N. J. Millam, M. Klene, J. E. Knox, J. B. Cross, V. Bakken, C. Adamo, J. Jaramillo, R. Gomperts, R. E. Stratmann, O. Yazyev, A. J. Austin, R. Cammi, C. Pomelli, J. W. Ochterski, R. L. Martin, K. Morokuma, V. G. Zakrzewski, G. A. Voth, P. Salvador, J. J. Dannenberg, S. Dapprich, A. D. Daniels, Ö. Farkas, J. B. Foresman, J. V. Ortiz, J. Cioslowski and D. J. Fox, *Gaussian 09, Revision B.01*, Gaussian, Inc., Wallingford CT, 2010.
- 29 Y. Zhao, N. E. Schultz and D. G. Truhlar, Exchange-Correlation Functional with Broad Accuracy for Metallic and Nonmetallic Compounds, Kinetics, and Noncovalent Interactions, *J. Chem. Phys.*, 2005, **122**, 161103.
- 30 Y. Zhao, N. E. Schultz and D. G. Truhlar, Design of Density Functionals by Combining the Method of Constraint Satisfaction with Parameterization for Thermochemistry, Thermochemical Kinetics, and Noncovalent Interactions, *J. Chem. Theory Comput.*, 2006, **2**, 364–382.
- 31 P. D. Patel and A. E. Masunov, Theoretical Study of Photochromic Compounds. 1. Bond Length Alternation and Absorption Spectra for the Open and Closed Forms of 29 Diarylethene Derivatives, *J. Phys. Chem. A*, 2009, **113**, 8409–8414.
- 32 I. H. M. van Stokkum, D. S. Larsen and R. van Grondelle, Global and Target Analysis of Time-Resolved Spectra, *Biochim. Biophys. Acta, Bioenerg.*, 2004, **1657**, 82–104.
- 33 W. Al-Soufi, M. Novo, M. Mosquera and F. Rodriguez-Prieto, Principle Component Global Analysis of Series of Fluorescence Spectra, in *Reviews in Fluorescence 2009*, ed. G. D. Geddes, Springer, 2011, vol. XII, pp. 23–45.
- 34 Y. Harabuchi, K. Keipert, F. Zahariev, T. Taketsugu and M. S. Gordon, Dynamics Simulations with Spin-Flip Time-Dependent Density Functional Theory: Photoisomerization and Photocyclization Mechanisms of *cis*-Stilbene in $\pi\pi^*$ States, *J. Phys. Chem. A*, 2014, **118**, 11987–11998.
- 35 T. Nakamura, S. Takeuchi, T. Taketsugu and T. Tahara, Femtosecond fluorescence study of the reactions pathways and nature of the reactive S_1 state of *cis*-stilbene, *Phys. Chem. Chem. Phys.*, 2012, **14**, 6225–6232.
- 36 S. T. Repinec, R. J. Sension, A. Z. Szarka and R. M. Hochstrasser, Femtosecond Laser Studies of the *cis*-Stilbene Photoisomerization Reactions: the *cis*-Stilbene to Dihydrophenanthrene Reaction, *J. Phys. Chem.*, 1991, **95**, 10380–10385.
- 37 R. J. Sension, S. T. Repinec, A. Z. Szarka and R. M. Hochstrasser, Femtosecond Laser Studies of the *cis*-Stilbene Photoisomerization Reactions, *J. Chem. Phys.*, 1993, **98**, 6291–6315.
- 38 J.-M. Rodier and A. B. Myers, *cis*-Stilbene Photochemistry: Solvent Dependence of the Initial Dynamics and Quantum Yields, *J. Am. Chem. Soc.*, 1993, **115**, 10791–10795.
- 39 M. Quick, A. L. Dobryakov, I. N. Ioffe, F. Berndt, R. Mahrwald, N. P. Ernsting and S. A. Kovalenko, Rotamer-Specific Photoisomerization of Difluorostilbenes from Transient Absorption and Transient Raman Spectroscopy, *J. Phys. Chem. B*, 2018, **122**, 1049–1059.
- 40 D. Grebner, M. Helbing and S. Rentsch, Size-Dependent Properties of Oligothiophenes by Picosecond Time-Resolved Spectroscopy, *J. Phys. Chem.*, 1995, **99**, 16991–16998.
- 41 R. Rossi, M. Ciofalo, A. Carpitia and G. Ponterini, Singlet-triplet intersystem crossing in 2,2':5',2''-terthiophene and some of its derivatives, *J. Photochem. Photobiol., A*, 1993, **70**, 59–67.
- 42 R. S. Becker, J. Seixas de Melo, A. L. Maçanita and F. Elisei, Comprehensive Evaluation of the Absorption, Photophysical, Energy Transfer, Structural and Theoretical Properties of α -Oligothiophenes with One to Seven Rings, *J. Phys. Chem.*, 1996, **100**, 18683–18695.
- 43 T. Fukaminato, T. Kawai, S. Kobatake and M. Irie, Fluorescence of Photochromic 1,2-Bis(3-methyl-2-thienyl)ethene, *J. Phys. Chem. B*, 2003, **107**, 8372–8377.
- 44 N. J. Turro, V. Ramamurthy and J. C. Scaiano, *Modern molecular photochemistry of organic molecules*, University Science, Sausalito, Calif., 2004.